Multicritical phase diagram of PrMn$_{1-x}$Sb$_2$ with two interacting magnetic elements

Takahiro Urata [1,*] Yusuke Takahashi,[1] Kentaro Kuga [2] Tsunehiro Takeuchi [2] and Hiroshi Ikuta [1]

[1]*Department of Materials Physics, Nagoya University, Chikusa-ku, Nagoya 464-8603, Japan*
[2]*Toyota Technological Institute, Tempaku-ku, Nagoya 468-8511, Japan*

We carried out systematic magnetotransport measurements to study the magnetic phase diagram of PrMn$_{1-x}$Sb$_2$, where two antiferromagnetic orders associated with the moments of Pr and Mn coexist. When the magnetic field (H) was applied parallel to the crystallographic c axis, we found a tricritical point where a first-to-second order changeover takes place as in ordinary metamagnets. On the other hand, the metamagnetic transition field decreased unexpectedly with decreasing the temperature at low temperatures for $H \parallel [110]$. Further, the transition line associated with the metamagnetic transition terminated at low temperature, where a multicritical point was formed. Starting from a three-dimensional phase diagram predicted from a simple model and modifying it to fit our experimental results, we argue that the magnetic interaction between the two magnetic elements is responsible for forming the new critical point and influences the shape of the phase boundaries.

I. INTRODUCTION

A wide variety of physical systems exhibit intriguing multicritical phase diagrams that have been the subject of considerable interest [1,2]. It is well known that a tricritical point exists on the magnetic field (H)–temperature (T) phase diagram of an anisotropic antiferromagnet when it undergoes a metamagnetic transition [3]. In a mixed system of two materials that have different magnetic anisotropy, a tetracritical point exists on the component-temperature phase diagram where two transition lines intersect [4–6]. The tetracritical point in these compounds was attributed to the randomness inherent to a mixed compound system [7,8] because renormalization-group theories predicted the absence of a tetracritical point in a system with spin degrees of freedom of less than four ($n < 4$) [9,10]. However, recent soft x-ray magnetic circular dichroism (XMCD) studies revealed the existence of a tetracritical point on the H-T phase diagram of MnCr$_2$S$_4$ [11,12]. As it is a line compound with no randomness and three spin degrees of freedom ($n = 3$), this finding prompted reconsideration of the theory and led to a proposal of a new mechanism based on spin-lattice coupling in a frustrated system [12], which demonstrated that compounds with multiple magnetic elements may harbor unexplored and interesting physics.

In previous work, we studied the magnetic phase diagram of PrMnSb$_2$ [13], which has two antiferromagnetic sublattices. Upon cooling under zero magnetic field, first Mn moments order at $T_N^I \approx 190$ K (phase I) and then Pr moments at $T_N^{II} \approx 32$ K (phase II) [13,14]. In the ordered states, Mn moments are aligned predominantly along [110], while Pr moments along the c-axis direction [see Fig. 1(a) for the crystal and magnetic structures]. The results of our magnetization measurements indicated that the magnetic anisotropy was rather strong as both phases underwent a metamagnetic

transition [13]. Phase I exhibited a metamagnetic transition when a magnetic field was applied parallel to the crystallographic *ab* plane. The transition took place at a lower field for $H \parallel [110]$ than $H \parallel [100]$, reflecting the in-plane anisotropy of the Mn moments. Phase II also displayed a metamagnetic transition but for $H \parallel [001]$, which indicates it is associated with the Pr sublattice, considering the magnetic anisotropy.

In addition, PrMnSb$_2$ was found to be electrically conductive [13], which allows us to study the multicritical phenomena through transport measurements. There are other antiferromagnets that have two magnetic elements and are conductive, such as EuFe$_2$As$_2$ and EuMnX_2 ($X =$ Sb or Bi). However, in these materials, only the Eu sublattice undergoes a metamagnetic or spin-flop transition at a finite magnetic field but not the 3d element sublattice [15–17], which is reasonable because the magnetic anisotropy of 3d elements is usually small. PrMnSb$_2$ is therefore a rather rare system that shows metamagnetic transitions attributable to each magnetic sublattice and is electrically conductive.

The phase diagram constructed in our previous study was based on magnetization data and did not include information about the nature of the transitions. Here, we carried out a detailed study on the phase diagram of PrMnSb$_2$ by systematically measuring the magnetoresistance effect. The results revealed the existence of an unexpected multicritical point (MCP) for $H \parallel [110]$. By considering a three-dimensional phase diagram, we argue that the new MCP emerged because the first-to-second order changeover (FSOC) line was deformed to conform to the Gibbs phase rule in a system with two interacting magnetic elements.

II. EXPERIMENT

Single crystals of PrMn$_{1-x}$Sb$_2$ were grown by a Sn-flux method [13]. The largest sample surface was confirmed to be the (001) plane by out-of-plane x-ray diffraction. The chemical compositions of the samples were determined by

*Corresponding author: urata@mp.pse.nagoya-u.ac.jp
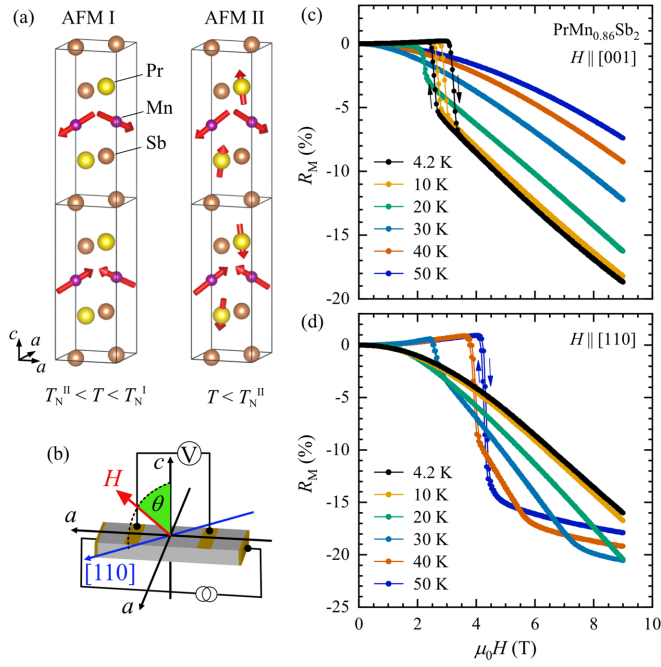
FIG. 1. (a) The crystal and magnetic structures of PrMnSb$_2$ at $T_N^{II} < T < T_N^{I}$ (left) and $T < T_N^{II}$ (right) drawn by VESTA [30]. The black frames represent a unit cell for origin choice 2 of $P4/nmm$ of the International Tables of Crystallography. (b) A schematic illustration of the measurement setup. (c), (d) The magnetic field dependence of magnetoresistance ratio measured at various temperatures. The magnetic field was applied parallel to (c) the c axis and (d) [110]. Hysteresis was observed at (c) low and (d) high temperatures as indicated by arrows. Only data of representative temperatures are shown and the complete data set is reported in the Supplemental Material [20].

energy-dispersive x-ray spectroscopy. Mn was slightly deficient, similarly to earlier studies on polycrystalline samples [14,18,19]. The transport properties were measured by a conventional four-terminal method using a physical property measurement system (PPMS), Quantum Design. The current was supplied parallel to the a axis for all measurements reported here. Heat capacity was measured by a thermal relaxation method using a PPMS.

III. RESULTS AND DISCUSSION

Figures 1(c) and 1(d) show the magnetic field dependence of magnetoresistance ratio (R_M) at various temperatures. The sample had a chemical composition of PrMn$_{0.86}$Sb$_2$. For clarity, we show only the data of representative temperatures in these figures, and the complete data set can be found in the Supplemental Material [20]. The magnetoresistance ratio is defined as $R_M = 100\% \times [\rho(H) - \rho(0)]/\rho(0)$, where ρ denotes the resistivity. The measurement setup is schematically depicted in Fig. 1(b). The magnetic field was rotated within the [001]-[110] plane, where θ indicates the angle between the c axis and the magnetic field. For $H \parallel [001]$ ($\theta = 0$), R_M decreased monotonically with H at high temperatures ($T > T_N^{II}$) as shown in Fig. 1(c). The reduction in the magnetic scattering by aligning unordered Pr moments with the magnetic field
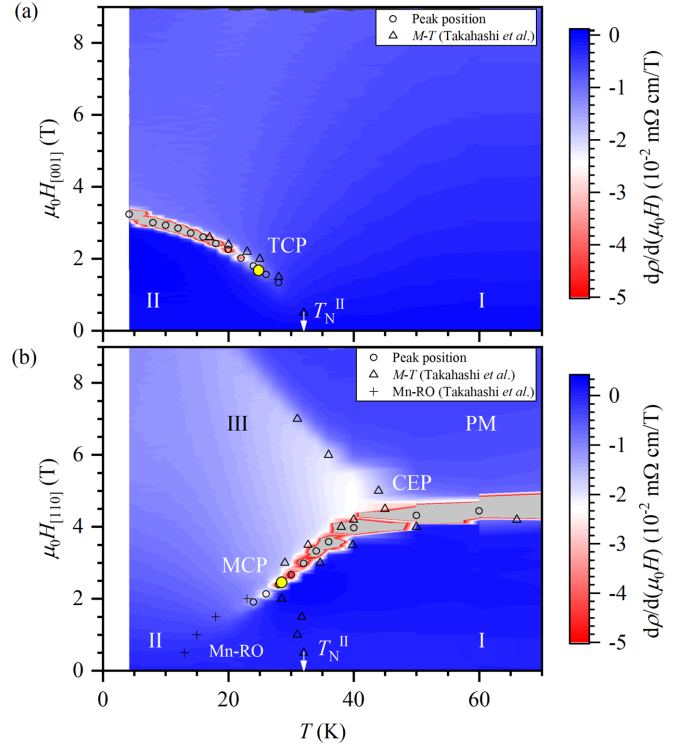
FIG. 2. Color maps of the first derivative of resistivity [$d\rho/d(\mu_0 H)$] depicted on the H-T plane. Locations where the value was below the range of the color scale are indicated by gray. The magnetic field was applied along (a) the c axis and (b) [110]. The open circles indicate the peak positions in the field dependence of $-d\rho/d(\mu_0 H)$. The open triangles show the transition temperature and the crosses the boundary of the Mn-reorientation (Mn-RO) region both deduced from the temperature dependence of magnetization by Takahashi *et al.* [13].

is probably the reason for the negative magnetoresistance effect. On the other hand, a sharp drop was observed at lower temperatures, and a hysteresis was also evident. These sharp magnetoresistance changes are attributable to the metamagnetic transition between the Pr ordered (phase II) and the Pr unordered phases.

Figure 1(d) shows the data for $H \parallel [110]$ ($\theta = 90°$). Here, we also observed a steep resistivity drop with increasing the magnetic field, but only in the temperature range of phase I. Therefore, the resistivity drop should be associated with the metamagnetic transition of the Mn sublattice. At temperatures below T_N^{II}, the magnetoresistance decreased monotonically with increasing H, which may have been caused by a small rotation of the Pr and/or Mn moments.

The color map in Fig. 2(a) represents the first derivative of resistivity with respect to the magnetic field for $H \parallel [001]$. The first derivative was calculated from the resistivity data measured with field ascending. At low temperatures, the first derivative had a large negative value at the metamagnetic transition because of the sharp resistivity drop, and the circles indicate where $-d\rho/d(\mu_0 H)$ recorded a peak (i.e., where the ρ-H curve had the steepest slope). The triangles show the phase boundary determined from the temperature dependence of magnetization (M-T) in our previous work [13], which is in

good agreement with the present study. The boundary between phases I and II can be clearly defined at low temperatures, but gradually fades out toward higher temperatures. This means that the transition between the two phases is of first order at low temperatures and second order at high temperatures, consistent with a typical metamagnetic transition seen in anisotropic antiferromagnets [3]. The point where the FSOC takes place is a tricritical point (TCP) [3,21]. We applied a tricritical scaling analysis to the magnetization data (see the Supplemental Material [20] and Refs. [22,23] therein), which gave a tricritical temperature of 25 K as indicated by a yellow dot in Fig. 2(a).

Figure 2(b) shows the color map similarly constructed for $H \parallel [110]$. The transition from phase I to the paramagnetic (PM) state at $T \gtrsim 50$ K is abrupt, and the boundary is well defined. The transition is therefore first order in this temperature range as expected because it is well below the Néel temperature of the Mn sublattice ($T_N^I \approx 190$ K). In an ordinary antiferromagnet, the metamagnetic transition should remain first order and the transition field should increase as the temperature is lowered. However, we observed an unexpected behavior at $T \lesssim 50$ K; i.e., the first-order transition line changed the slope and the transition field decreased with decreasing the temperature. Further, the transition became less distinct at low temperatures, suggesting the presence of an FSOC and an associated critical point. The magnetization data showed a similar behavior, to which we applied a tricritical scaling analysis. The scaling held fairly well as shown in the Supplemental Material [20] and gave a tricritical temperature of 28.5 K as indicated by a yellow dot in Fig. 2(b).

Bordering to the first-order transition line, a white-colored section that fans out from about 50 K to lower temperatures is evident in Fig. 2(b). This white region corresponds to where R_M decreased almost linearly with H above the metamagnetic transition field before the field dependence became weaker [see, e.g., the 40 K data in Fig. 1(d)]. The boundary between the fan-shaped region and the PM phase coincides with the transition line determined from the M-T measurements [13] and terminates where it meets the first-order transition line, forming a critical end point (CEP). The fan-shaped region corresponds to the region that we assigned to phase II in our previous work. In phase II, both Mn and Pr moments order antiferromagnetically [14]. In the present study, however, we observed a clear metamagnetic transition associated with the Mn sublattice down to at least $T \sim 30$ K, indicating that the Mn moments are not ordered above the transition field. Hence, there must be a region where only Pr moments are ordered apart from phase II. This new phase will be referred to as phase III hereafter. Note that a boundary between phases II and III should exist in the white fan-shaped region, but it could not be established with the present experiments. Probably, a method more sensitive to changes in the magnetic structure might detect the transition between the two phases, such as neutron diffraction or XMCD.

As pointed out above, our results revealed an FSOC-like behavior at low temperature for $H \parallel [110]$. We note though that there is a difference from a normal FSOC. If this point merely signals an order changeover, the metamagnetic transition line extended to lower temperatures should represent a second-order transition. In fact, we have observed
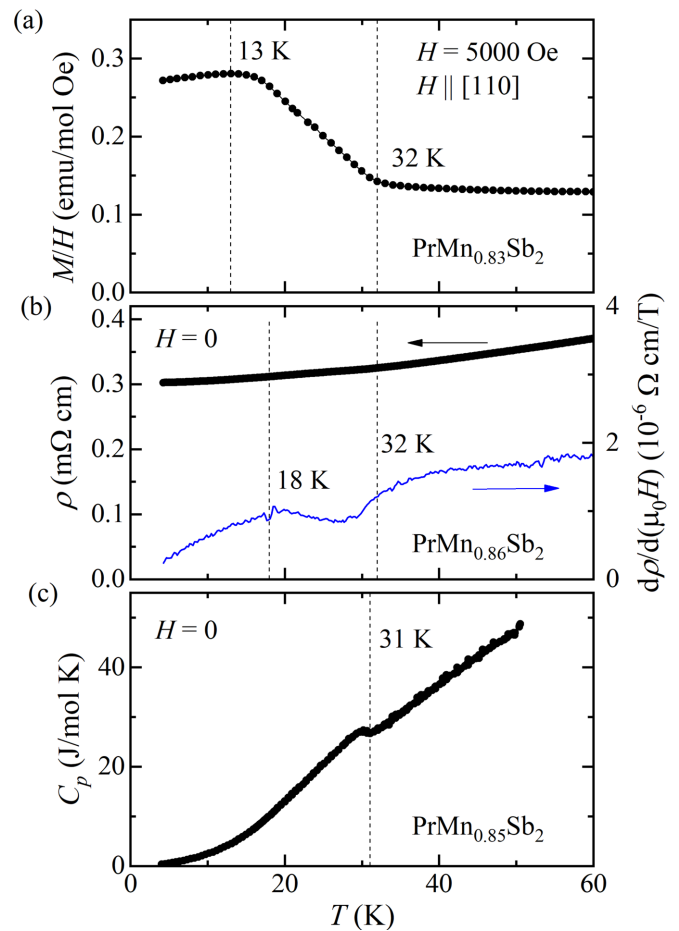
FIG. 3. The temperature dependence of (a) normalized magnetization, (b) resistivity (black) and its temperature derivative (blue), and (c) heat capacity. The samples used in these measurements had slightly different Mn deficiencies, and the analytically determined compositions are shown in the panels. Panels (a) and (b) are expanded views at low temperature of the data reported in our previous work [13]. For the heat capacity measurement, we used a stack of several crystals and the average composition is indicated in the panel.

anomalies in the temperature dependence of magnetization and resistivity in this temperature range as reported in our previous work [13], the low-temperature parts of which are reproduced in Figs. 3(a) and 3(b). However, a neutron scattering study has reported only two magnetic phases (phases I and II), although the canting angles of the Mn moments were slightly different at 70 and 10 K [14]. Therefore, we concluded that the observed magnetization and resistivity anomalies are due to small reorientation of Mn moments [13]. To further check whether there are no other phase transitions, we measured the heat capacity in the present study. The result indeed rules out the Mn-reorientation (Mn-RO) region as a separate thermodynamic phase because no distinct change in the temperature dependence is seen below T_N^{II} as shown in Fig. 3(c). Therefore, the boundary between phase II and the Mn-RO region is rather like a Widom line observed in supercritical fluids [24,25], and the thermodynamic transition line terminates at the FSOC-like point.
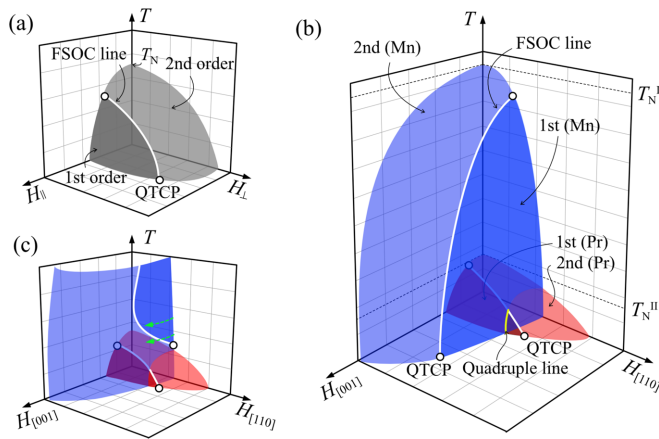
FIG. 4. (a) A schematic phase diagram in three dimensions expected from an antiferromagnetic Ising model [26,27]. $H_\parallel$ and $H_\perp$ indicate the longitudinal and transverse fields, respectively. (b) A phase diagram expected for PrMnSb$_2$ if there were no interaction between Pr and Mn moments, and (c) that with a deformed FSOC line to avoid the formation of a quadruple line. The transition surfaces of the Pr and Mn sublattices are depicted in red and blue, respectively, and QTCP stands for quantum tricritical point. Only the low-temperature part is shown in (c), where it differs from (b), and the green dashed arrows correspond to those of Figs. 5(a) and 5(b).

There is also an ambiguity in how many transition lines meet at the FSOC-like point. At least, the boundary between phase I and the Mn-RO region seems to meet the metamagnetic transition line here, but it is also possible it joins with the boundary between phases II and III. The latter could not be detected experimentally as mentioned above, but must exist around here. The nature of the FSOC-like point remains therefore an open question for future work and we denoted it simply as MCP in Fig. 2(b).

In order to gain insight into why the new MCP has emerged, we extend the phase diagram to three dimensions (3D). The transition between the ordered and paramagnetic states in a simple antiferromagnet is first (second) order at low (high) temperatures under longitudinal magnetic fields ($H_\parallel$), while it is second order over the entire temperature range under transverse magnetic fields ($H_\perp$) [26,27]. Hence, a typical phase diagram in 3D can be drawn as Fig. 4(a). The FSOC points form a line in 3D, which is drawn in white. The transition surface, the phase boundary in 3D, drawn in dark (light) gray represents a first (second)–order transition. A quantum tricritical point (QTCP) is expected where the FSOC line ends at zero temperature [27]. Note that the first experimental observation of a QTCP was recently reported in the study of the field-temperature-composition phase diagram of Nb$_{1-y}$Fe$_{2+y}$ [28].

If PrMnSb$_2$ were a simple two-magnetic-sublattice system, the 3D phase diagram would be a superposition of two such diagrams of Fig. 4(a). Accounting for the magnetic anisotropy of each sublattice, the phase diagram expected for PrMnSb$_2$ would be like Fig. 4(b). The red and blue transition surfaces correspond to the Pr and Mn sublattices, respectively. It is notable that there is an intersection of the two first-order transition surfaces, which is drawn in yellow. Because two phases

coexist at a first-order transition, four phases coexist at this yellow line, making it a quadruple line. This does not violate the Gibbs phase rule as it allows a line of four coexisting phases for a two-component system with three variables [29]. However, if there is non-negligible interaction between Pr and Mn moments, they cannot be considered as two independent components and the formation of a quadruple line is prohibited. One way to avoid this is to deform the Mn FSOC line as depicted in Fig. 4(c) because then the Mn transition is second-order where the two transition surfaces intersect. This is likely the case because the deformed FSOC line meets the $H_{[001]} = 0$ plane at two points, the one at lower temperature corresponding to where we observed a FSOC-like change on the $H_{[001]} = 0$ plane [Fig. 2(b)]. In the following, we make a more detailed comparison of Fig. 4(c) and the experimental results.

Figures 5(a)–5(e) show the first derivative of R_M with respect to the magnetic field at various temperatures depicted on the ($H_{[110]}$, $H_{[001]}$) plane, where $H_{[110]} = H\sin(\theta)$ and $H_{[001]} = H\cos(\theta)$. The R_M data were taken at every 5° in the range of $0° \leqslant \theta \leqslant 90°$ [see Fig. 1(b)]. These figures correspond to the constant-temperature slices of the 3D phase diagram. The $dR_M/d(\mu_0 H)$-H curves used to construct these figures are shown in Fig. S5 of the Supplemental Material [20]. The peak positions of the magnetic field dependence of $-dR_M/d(\mu_0 H)$ are indicated by open circles. Clearly, the ($H_{[110]}$, $H_{[001]}$) space is divided into several phases depending on the temperature.

At 50 K, only the Mn sublattice is ordered and undergoes a metamagnetic transition. Because the Mn moments are oriented predominantly along [110], the metamagnetic transition field is expected to depend primarily on $H_{[110]}$ [26,27]. Consistent with the expectation, the phase boundary between phase I and the paramagnetic region runs almost vertically in Fig. 5(a). The phase boundary at low $H_{[001]}$ is very sharp indicative of a first-order transition but becomes somewhat blurred with increasing $H_{[001]}$ and the phase transition is second-order-like. Similarly, the transition line of the Mn-ordered phase (phase I) runs vertically at 35 K as shown in Fig. 5(b). Interestingly, the transition becomes blurred at a lower $H_{[001]}$ at 35 K than at 50 K. This is inconsistent with Fig. 4(b), where the region of first-order transition is wider at lower temperatures, but consistent with Fig. 4(c) owing to the deformed FSOC line [see the two green arrows in Fig. 4(c)]. Moreover, a new transition line is evident at 35 K, which meets that of phase I at ($\mu_0 H_{[110]}$, $\mu_0 H_{[001]}$) $\approx$ (3.9, 3.9). The region surrounded by the two transition lines can be assigned to phase III from the comparison with Fig. 2(b), which means that phase III overhangs above T_N^{II} (32 K). This feature is not represented in the phase diagram of Fig. 4(c) and the necessary amendment will be discussed below.

At 25 K, the phase boundaries are less distinct and hence more second-order-like as shown in Fig. 5(c). At this temperature, which is lower than T_N^{II} (32 K), both Pr and Mn are ordered at low fields (phase II). Although faintly, the boundary enclosing phase II is noticeable. With further decreasing the temperature to 15 K, the boundary between phases I and II and that between phases III and PM get noticeably sharper. These transition lines run almost horizontally because Pr moments order nearly parallel to the c axis in phases II and III. Similar
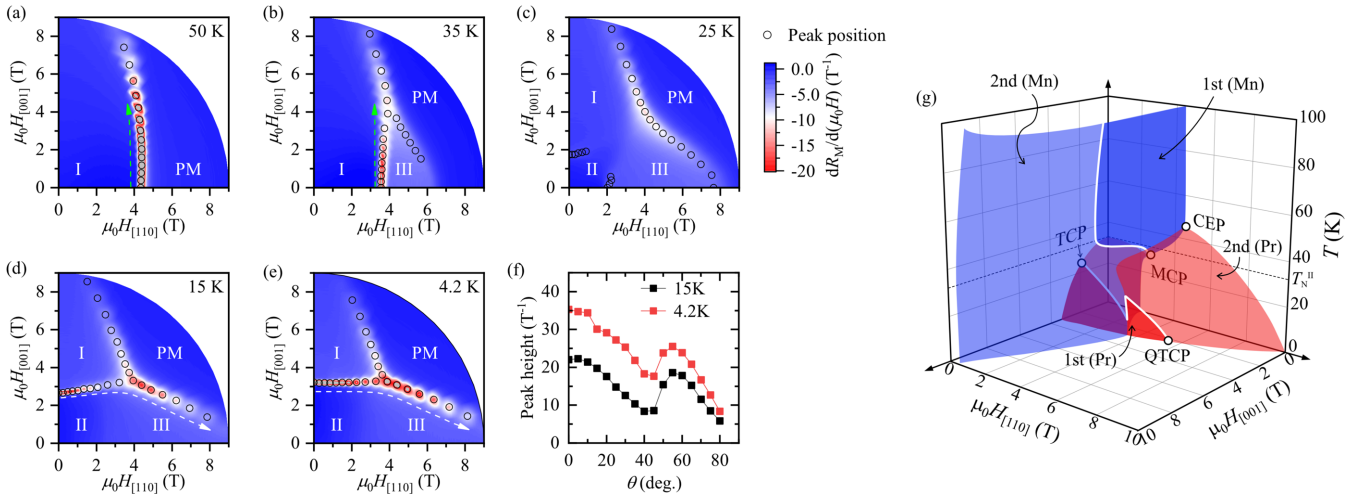
FIG. 5. (a)–(e) Color maps of the first derivative of magnetoresistance ratio $[dR_M/d(\mu_0 H)]$ depicted on the $H_{[110]}$-$H_{[001]}$ plane. Locations where the value is below the lower limit of the scale are indicated by gray. The open circles indicate the peak positions in the field dependence of $-dR_M/d(\mu_0 H)$. (f) The peak height of $-dR_M/d(\mu_0 H)$ along the Pr transition lines indicated by the dashed white arrows in (d) and (e) as a function of the field angle. (g) A schematic phase diagram in three dimensions summarizing our observations. TCP, CEP, and MCP correspond to those of Fig. 2.

to the phase transition line of the Mn sublattice at 50 K, the Pr transition line becomes blurry at high fields. The phase diagram at 4.2 K is similar to that at 15 K.

Figure 4(c) accounts for the essential features of our data reasonably well, except that the region of phase III extends to above T_N^{II} for $H \parallel [110]$. A possible amendment to conform the 3D phase diagram to this observation is slicing the Pr transition surface and lifting the outer part as shown in Fig. 5(g). If this is the case, an intriguing consequence is that the FSOC line on the Pr transition surface has a zigzag shape. Figure 5(f) plots the $-dR_M/d(\mu_0 H)$ value along the Pr transition lines indicated by the white dashed arrows in Figs. 5(d) and 5(e) as a function of $\theta = \arctan(H_{[110]}/H_{[001]})$. The angle dependence is nonmonotonic with a local minimum at an intermediate angle (40°–45°), which may indicate a swinging between first-order and second-order transition in accordance with the zigzag shape of the FSOC line. We therefore think Fig. 5(g) captures most accurately the experimental results of the present study. The magnetic interaction between Pr and Mn is probably the reason why the transition surface is deformed as Fig. 5(g), but the detailed mechanism is far from well understood. It is highly desirable that future theoretical studies would address this issue.

IV. CONCLUSION

In conclusion, we constructed field-temperature (H-T) phase diagrams of PrMn$_{0.86}$Sb$_2$ from magnetoresistance measurements. For $H \parallel [001]$, a tricritical point was observed similarly to ordinary metamagnets, but the phase diagram for $H \parallel [110]$ was quite different and revealed the presence of a new MCP. The discussion about the phase diagram in three dimensions showed that the formation of this MCP can be understood as a result of conforming to the phase rule in a system with two interacting magnetic elements. We stress that the magnetic phases in this system can be controlled by simply changing the direction of the applied magnetic field and provide an intriguing platform for studying the physics of multicritical phenomena arising from coupled magnetic orders.

[1] R. Pynn and A. Skjeltorp, editors, *Multicritical Phenomena*, NATO ASI Series B: Physics, Vol. 106 (Plenum Press, 1984).

[2] A. Aharony, J. Stat. Phys. **110**, 659 (2003).

[3] E. Stryjewski and N. Giordano, Adv. Phys. **26**, 487 (1977).

[4] K. Katsumata, M. Kobayashi, and H. Yoshizawa, Phys. Rev. Lett. **43**, 960 (1979).

[5] P.-z. Wong, P. M. Horn, R. J. Birgeneau, C. R. Safinya, and G. Shirane, Phys. Rev. Lett. **45**, 1974 (1980).

[6] A. N. Pirogov, J.-G. Park, A. S. Ermolenko, A. V. Korolev, A. G. Kuchin, S. Lee, Y. N. Choi, J. Park, M. Ranot, J. Yi,

E. G. Gerasimov, Y. A. Dorofeev, A. P. Vokhmyanin, A. A. Podlesnyak, and I. P. Swainson, Phys. Rev. B **79**, 174412 (2009).

[7] S. Fishman and A. Aharony, Phys. Rev. B **18**, 3507 (1978).

[8] D. Mukamel, Phys. Rev. Lett. **46**, 845 (1981).

[9] M. E. Fisher and D. R. Nelson, Phys. Rev. Lett. **32**, 1350 (1974).

[10] J. M. Kosterlitz, D. R. Nelson, and M. E. Fisher, Phys. Rev. B **13**, 412 (1976).

[11] A. Miyata, H. Suwa, T. Nomura, L. Prodan, V. Felea, Y. Skourski, J. Deisenhofer, H.-A. Krug von Nidda, O. Portugall,

S. Zherlitsyn, V. Tsurkan, J. Wosnitza, and A. Loidl, Phys. Rev. B **101**, 054432 (2020).

[12] S. Yamamoto, H. Suwa, T. Kihara, T. Nomura, Y. Kotani, T. Nakamura, Y. Skourski, S. Zherlitsyn, L. Prodan, V. Tsurkan, H. Nojiri, A. Loidl, and J. Wosnitza, Phys. Rev. B **103**, L020408 (2021).

[13] Y. Takahashi, T. Urata, and H. Ikuta, Phys. Rev. B **104**, 054408 (2021).

[14] S. K. Malik, Z. Chu, A. G. Joshi, J. B. Yang, W. B. Yelon, Q. Cai, W. J. James, and K. Kamaraju, J. Appl. Phys. **91**, 7842 (2002).

[15] S. Jiang, Y. Luo, Z. Ren, Z. Zhu, C. Wang, X. Xu, Q. Tao, G. Cao, and Z. Xu, New J. Phys. **11**, 025007 (2009).

[16] C. Yi, S. Yang, M. Yang, L. Wang, Y. Matsushita, S. Miao, Y. Jiao, J. Cheng, Y. Li, K. Yamaura, Y. Shi, and J. Luo, Phys. Rev. B **96**, 205103 (2017).

[17] A. F. May, M. A. McGuire, and B. C. Sales, Phys. Rev. B **90**, 075109 (2014).

[18] O. Sologub, K. Hiebl, P. Rogl, and O. Bodak, J. Alloys Compd. **227**, 40 (1995).

[19] P. Wollesen, J. Jeitschko, M. Bylak, and L. Dietrich, J. Alloys Compd. **245**, L5 (1996).

[20] See Supplemental Material at http://link.aps.org/supplemental/10.1103/PhysRevB.106.184401 for detailed magnetoresistance data and critical scaling of magnetization data.

[21] R. B. Griffiths, Phys. Rev. Lett. **24**, 715 (1970).

[22] R. B. Griffiths, Phys. Rev. B **7**, 545 (1973).

[23] N. Giordano and W. P. Wolf, AIP Conf. Proc. **29**, 459 (1976).

[24] B. Widom, in *Phase Transitions and Critical Phenomena*, Vol. 2, edited by C. Domb and M. S. Green (Academic Press, 1972).

[25] G. G. Simeoni, T. Bryk, F. A. Gorelli, M. Krisch, G. Ruocco, M. Santoro, and T. Scopigno, Nat. Phys. **6**, 503 (2010).

[26] G. Wei, J. Liu, H. Miao, and A. Du, Phys. Rev. B **76**, 054402 (2007).

[27] Y. Kato and T. Misawa, Phys. Rev. B **92**, 174419 (2015).

[28] S. Friedemann, W. J. Duncan, M. Hirschberger, T. W. Bauer, R. Küchler, A. Neubauer, M. Brando, C. Pfleiderer, and F. Grosche, Nat. Phys. **14**, 62 (2018).

[29] J. W. Gibbs, *Scientific Papers: Thermodynamics* (Dover Publications, 1961).

[30] K. Momma and F. Izumi, J. Appl. Crystallogr. **44**, 1272 (2011).